Optimal pose selection for vision-based kinematic calibration of parallel mechanisms

Pierre Renaud[1], Nicolas Andreff[1], Grigore Gogu[1], Michel Dhome[2]

[1]*LaRAMA, U. Blaise Pascal/IFMA, Clermont-Ferrand, France,* {renaud|andreff|gogu}@ifma.fr
[2]*LASMEA, U. Blaise Pascal/CNRS, Clermont-Ferrand, France,* dhome@lasmea.univ-bpclermont.fr

Abstract

In this paper, a new pose selection criterion for the kinematic calibration of parallel mechanisms is proposed. It enables one to take into account the measurement noise amplification that may occur for parallel mechanisms, as well as the variation of amplitude and anisotropy of the measuring device accuracy. This new criterion is applied to vision-based calibration of an Orthoglide mechanism, both in simulation, with comparison to existing criteria, and experimentally.

1 Introduction

Compared to serial mechanisms, parallel structures may exhibit a much better repeatability [1], but their large number of links and passive joints often limits their performance in terms of accuracy [2]. A kinematic calibration is thus needed. For such structures, the inverse kinematic model can usually easily be derived [1]. One method to perform calibration of a parallel structure is then to minimize an error between the measured joint variables and their corresponding values, estimated from the measured end-effector pose and the inverse kinematic model [3]. This method seems to be the most numerically efficient among the calibration algorithms for parallel structures [4]. Nevertheless, it is constrained by the need for accurate measurement of the full end-effector pose (*i.e.* both its position and its orientation). Some adapted measuring devices have been proposed : laser tracking systems [5], mechanical devices [6] or vision-based systems [7]. One might notice that they all demonstrate an inhomogeneous accuracy in the measurement volume.

Determining the kinematic parameter values with a good numerical accuracy requires to adequately choose a set of mechanism configurations, which can be related to the exciting trajectory problem [8]. Moreover, the parameter determination accuracy is also related to the influence of the measurement uncertainties. Indeed, the measurement noise is amplified according to the numerical stability of the identification algorithm, when applied to a set of measured end-effector poses. The pose selection strategy for calibration has therefore a strong influence on the identification efficiency, and this strategy must include measurement errors. Nevertheless, we did not find in the literature a pose selection criterion doing the latter in a satisfying way. In this paper, we hence investigate the influence of measurement errors in the context of parallel mechanisms, in order to propose a new pose selection criterion to achieve kinematic calibration.

In the second section, a brief state of the art on numerical issues related to parallel robot kinematic calibration is given, with focus on the pose selection criteria proposed in the literature. A new pose selection criterion is then introduced in the third section, based on the influence analysis of the kinematic singularities and the measurement accuracy. In the fourth section, the use of the proposed criterion is justified by simulation results on an Orthoglide mechanism. Finally, in the fifth section, some experimental results on an Orthoglide prototype [9] are presented.

2 State of the art

2.1 Identification cost function

Contrary to serial mechanisms, the inverse kinematic model of parallel mechanisms can often be expressed analytically [1]. It computes the joint variables $\mathbf{q}_c$ as a function of the end-effector pose $\mathbf{X}$ and the kinematic parameter vector ξ. Zhuang *et al.* proposed [3] to form, for any pose $\mathbf{X}_i$, the following error

$$\epsilon_i = \tilde{\mathbf{q}}_i - \mathbf{q}_c(\tilde{\mathbf{X}}_i, \xi) \tag{1}$$

between the corresponding measured joint values $\tilde{\mathbf{q}}_i$ and the computed ones $\mathbf{q}_c(\tilde{\mathbf{X}}_i, \xi)$, then to determine the kinematic parameters by measuring, with an exteroceptive sensor, N different poses $\tilde{\mathbf{X}}_i, i \in [1, N]$, and finally estimate ξ by the nonlinear minimization of the

following cost function with respect to ξ:

$$\chi^2(\xi) = \epsilon^T \epsilon, \quad \epsilon = (\epsilon_1^T, ..., \epsilon_N^T)^T \tag{2}$$

Wampler and Hollerbach [10] proposed an alternate identification cost function, using a maximum likelihood function. The *a priori* measurement accuracy and its influence on the parameter identification are taken into account simultaneously with the estimated variance of the kinematic parameters. However, for parallel mechanisms, kinematic parameters are often related to assembly operations. In such a context, *a priori* variance estimation of the parameters seems therefore very tedious. In the following we hence prefer not to use parameter variance estimation, and restrict ourselves to cost functions based on (2).

2.2 Cost function scaling

To increase the cost function efficiency, scaling of parameters ξ and error ϵ may be achieved [11].

Parameter scaling. The parameter values have to be scaled to improve the identification cost function conditioning. Among the proposed scaling factors, the extremal scaling value method [12] is the most often employed. This scaling is of great interest, because it is physically-based: it allows one to take into account the influence of the parameters ξ on the joint variable values.

Error scaling. A weighted identification cost function may be used to increase numerical efficiency:

$$\chi^2(\xi) = \epsilon^T \mathbf{W} \epsilon \tag{3}$$

It has been proposed [13] to use as a weighting matrix $\mathbf{W}$ the covariance matrix Σ_ϵ of the error estimated from the *a priori* measurement uncertainties.

Σ_ϵ is often chosen as a diagonal matrix so that the cost function (3) will be expressed by:

$$\chi^2(\xi) = {\epsilon_w}^T \epsilon_w \tag{4}$$

with $\Sigma_\epsilon = \mathbf{D}^T\mathbf{D}$ and $\epsilon_w = \mathbf{D}\epsilon$. The covariance matrix varies with the measurement poses.

2.3 Pose selection

The identification cost function is nonlinear with respect to the kinematic parameters. The Levenberg-Marquardt algorithm, very efficient numerically, can be implemented to solve for the parameters. Close to the identification cost function minimum, the algorithm is equivalent to a Gauss-Newton optimization method. From (4), the kinematic parameter vector ξ is then iteratively determined by solving the linear system :

$${\mathbf{J_P}}^T \mathbf{J_P} d\xi = {\mathbf{J_P}}^T \epsilon_w \tag{5}$$

where $\mathbf{J_P}$ is the Jacobian matrix of the error with respect to the kinematic parameters obtained by stacking the Jacobian matrices associated to each measured pose:

$$\mathbf{J_P}_i = \frac{\partial \epsilon_w(\mathbf{X}_i, \xi)}{\partial \xi}, i \in [1, N] \tag{6}$$

It is well-known that, provided that the linear system in (5) is not singular, its solution is uniquely obtained by

$$d\xi = \left(({\mathbf{J_P}}^T \mathbf{J_P})^{-1} {\mathbf{J_P}}^T \right) \epsilon_w \tag{7}$$

However, these results are not sufficient from the numerical point of view and it is necessary to handle error propagation. Indeed, in (7), ϵ_w is computed from the pose $\tilde{\mathbf{X}}$ measured with an exteroceptive sensor and the measured joint variable $\tilde{q}$. Due to measurement noise, an error $\delta\epsilon_w$ is introduced, which induces an error $\delta(d\xi)$ in the estimation of $d\xi$:

$$\frac{\|\delta(d\xi)\|}{\|d\xi\|} \leq Cond(\mathbf{J_P}) \frac{\|\delta\epsilon_w\|}{\|\epsilon_w\|} \tag{8}$$

with $Cond(\mathbf{J_P})$ the condition number of the Jacobian matrix $\mathbf{J_P}$, defined as the ratio $\sigma_{max}/\sigma_{min}$ between the extremal singular values, if this latter is not submitted to the influence of measurement noise. The criterion

$$C_1 = Cond(\mathbf{J_P}) \tag{9}$$

is therefore used as a pose selection criterion by several authors [14, 15, 16], since it is numerically more relevant than the simpler criterion based on the determinant [17]. Nahvi and Hollerbach [18] propose to use the ratio between the condition number and the smallest singular value σ_{min} of $\mathbf{J_P}$:

$$C_2 = \frac{\sigma_{max}}{\sigma_{min}^2} \tag{10}$$

This criterion is more efficient than C_1, as it enables one to simultaneously ensure the cost function sensitivity to the parameters [18] and reduce the measurement noise $\delta\epsilon_w$ influence, as $\delta(d\xi)$ and $\delta\epsilon_w$ are related by:

$$\|\delta(d\xi)\| \leq \frac{\sigma_{max}}{\sigma_{min}^2} \|\delta\epsilon_w\| \tag{11}$$

In the next section, we outline some deficiencies of these approaches, and propose a new pose selection criterion to optimize kinematic calibration of parallel mechanism using the inverse kinematic model.

3 A new pose selection criterion

3.1 Cost function selection

From a metrological point of view, pose determination is a complex process. Estimating the associated

measurement error statistical properties is therefore difficult. In particular, for a vision-based measuring device, the six pose components are determined simultaneously from a single calibration board image by a non-linear optimization process [19]. An evaluation of each pose component accuracy may be achieved, but the accurate determination of the whole corresponding pose measurement covariance matrix $\mathbf{W_X}$ seems too complex and tedious to estimate. The weighting matrix $\mathbf{W}$ in (3) is a function of $\mathbf{W_X}$. The lack of *a priori* knowledge of this latter matrix leads us to avoid the use of $\mathbf{W}$ and therefore to consider the standard least-squares cost function (2).

3.2 Pose selection criterion definition

A first-order approximation gives one the error $\delta\epsilon_i$ committed on the error ϵ_i as a function of the proprioceptive measurement noise $\mathbf{b}_q$ and exteroceptive noise $\mathbf{b}_X$:

$$\delta\epsilon_i \simeq \left(\mathbf{b}_q + \frac{\partial \mathbf{q}_c}{\partial \mathbf{X}}(\mathbf{X}_i, \xi)\mathbf{b}_X \right) \tag{12}$$

Thus, the exteroceptive measurement noise is amplified by the inverse Jacobian matrix $\mathbf{J_X} = \frac{\partial \mathbf{q_c}}{\partial \mathbf{X}}$. Moreover, serial singularities [20] may occur, *i.e.* $\frac{\partial \mathbf{X}}{\partial \mathbf{q_c}}$ is rank deficient, hence $\mathbf{J_X}$ may have infinite singular values. Near to such singularities, the exteroceptive measurement noise has therefore a strong influence on the identification cost function.

The error $\delta\epsilon$ is not taken into account in the criteria C_1 and C_2. The exteroceptive measurement noise amplification is therefore not handled. We propose then to select the poses for kinematic calibration by minimizing the criterion C_3, which quantifies the cost function sensitivity to the parameters and the measurement noise influence:

$$C_3 = \frac{\sigma_{max}}{\sigma_{min}^2} \|\delta\epsilon\|_{sup} \tag{13}$$

with

$$\|\delta\epsilon\|_{sup} = \sqrt{\sum_{i=1}^{N} \left(\mathbf{b}_{\mathbf{q}sup} + \left| \frac{\partial \epsilon(\mathbf{X_i}, \xi)}{\partial \mathbf{X}} \right| \mathbf{b}_{\mathbf{X}sup} \right)^2} \tag{14}$$

where the notation $|.|$ stands for element-wise absolute value and $\mathbf{b}_{\mathbf{q}sup}$ and $\mathbf{b}_{\mathbf{X}sup}$ may be either the maximum measurement uncertainty, or the value corresponding to a predetermined confidence interval.

C_3 includes C_2. The cost function sensitivity to the kinematic parameters is therefore taken into account. In the same time, the upper-bound $\|\delta\epsilon\|_{sup}$ of the $\delta\epsilon$ vector norm enables us to consider the measurement noise influence on the error function.

No covariance matrix is needed: the error upper-bound $\|\delta\epsilon\|_{sup}$ is only dependent on the measurement uncertainty of each component but not on the whole measurement covariance matrix. The criterion C_3 can therefore be computed from the *a priori* knowledge.

Moreover, the use of C_3 enables one also to take into account the noise amplitude variation in the working volume by considering $\mathbf{b}_{\mathbf{q}sup}$ and $\mathbf{b}_{\mathbf{X}sup}$ dependent on the pose.

3.3 Pose determination

Optimizing an experiment plan is a common issue in identification. Many algorithms have been proposed to construct an optimal plan according to a specified criterion. In this paper, the DETMAX algorithm has been used. It enables one a simple implementation [21, 16], even if it does not provide us with any formal guarantee of finding a global optimum.

4 Simulation results

The pose selection criterion is an upper-bound of the measurement uncertainty influence. In order to evaluate the calibration improvement bound to the use of the proposed criterion, some kinematic calibration simulations are performed.

In this section, we are aiming at finding the best pose set with respect to vision-based calibration of an Orthoglide mechanism. First, we recall the Orthoglide inverse kinematic model, then test two measurement configurations to evaluate the criterion interest.

4.1 Orthoglide parallel mechanism

Presentation. The Orthoglide mechanism [9] is a three degree of freedom in translation parallel mechanism. Three linear actuators (Figure 1) ensure the end-effector movement by means of articulated parallelograms. The aim is to select the poses to calibrate the prototype built at IRCCyN using a vision-based measuring device. This measuring system, developed at LASMEA [22], enables one to measure the pose of a calibration board with respect to the camera, one being mounted onto the end-effector and the other being fixed with respect to the mechanism base.

Modeling. The mechanism is composed of three kinematic chains. To reduce the parameterization, the joint locations on the base are expressed in the camera frame R_C (Figure 1). In the same way, the end-effector location is defined by the calibration board frame origin $\mathbf{M}$ position. The parallelograms are modeled by their equivalent links between the actuators and the end-effector. Three loop equations can then be expressed :

$$\|\mathbf{A_j B_j}\|^2 = \|\mathbf{A_j O} + \mathbf{OM} + \mathbf{MB_j}\|^2, \; j \in [1, 3] \tag{15}$$

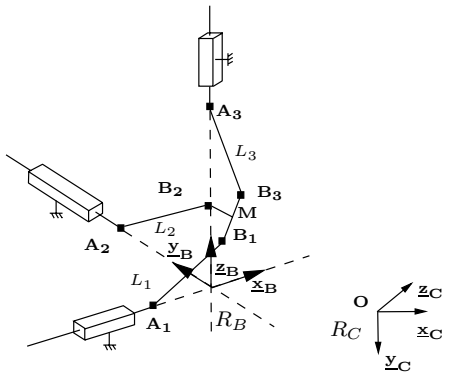

Figure 1: *The kinematic parameters of the Orthoglide mechanism.*

with **O** the camera center of projection. The left side of (15) is equal to the parallelogram length L_j. The right side is computed in the camera frame. The vector **OM** corresponds then to the measurement and one has:

$$\begin{aligned} \mathbf{A_jO} + \mathbf{MB_j} &= \mathbf{A_jA_{0j}} + \mathbf{A_{0j}O} + \mathbf{MB_j} \\ &= \mathbf{A_{0j}O} + \mathbf{MB_j} - \mathbf{q_j}\underline{\mathbf{u}}_j \end{aligned} \quad (16)$$

with $\mathbf{A_{0j}}$ the position of $\mathbf{A_j}$ when the joint encoder value is equal to zero, $\underline{\mathbf{u}}_j$ the unit vector defining the actuator orientation. One may notice that $\mathbf{A_{0j}O}$ and $\mathbf{MB_j}$ can only be identified by their sum $\mathbf{MB_j}'$ as they remain constant in the workspace. Six parameters are then necessary to define one kinematic chain: the length L_j, the $\mathbf{MB_j}'$ components and the angles ψ_j, θ_j defining the $\underline{\mathbf{u}}_j$ orientation.

The inverse kinematic model can then be expressed from the second-order in $\mathbf{q_j}$ equation:

$$\mathbf{q_j}^2 - 2R\mathbf{q_j} + S = 0 \quad (17)$$

with

$$\begin{aligned} R &= (x_{MB'_j} - X)\sin(\theta_j)\sin(\psi_j) \\ &\quad -(y_{MB'_j} - Y)\sin(\theta_j)\cos(\psi_j) + (z_{MB'_j} - Z)\cos(\theta_j) \\ S &= (x_{MB'_j} - X)^2 + (y_{MB'_j} - Y)^2 + (z_{MB'_j} - Z)^2 - L_j^2 \end{aligned}$$

The two solutions correspond to the two working modes, and selection is easily achieved.

With such a modeling, the three kinematic chains can be identified independently. For sake of clarity, only the kinematic calibration of the chain parallel to $\underline{\mathbf{x}}_\mathbf{B}$ (Figure 1) is detailed in the next paragraph. To identify the six kinematic parameters and ensure the solution uniqueness [23], a seven poses set is optimized.

4.2 First measurement configuration

In this first measurement configuration, the workspace corresponds to the one of the prototype. The simulated measurement accuracy results of a former evaluation of the vision-based measurement uncertainties [19]. The accuracy is linearly dependent on the distance between the camera, located outside the workspace, and the calibration board. The position measurement along the camera axis $\mathbf{z}_C$ is considered half as accurate as the other measurements, and accuracy varies between $0.13mm$ and $0.23mm$ in the mechanism workspace, in the $\underline{\mathbf{x}}_\mathbf{C}$ and $\underline{\mathbf{y}}_\mathbf{C}$ directions.

Table 1: *Pose optimization - Criteria values.*

Optimizer	C_2 val.	C_3 val.	E (mm)
First measurement configuration			
C_2	172	192	3.6
C_3	172	192	3.6
Second measurement configuration			
C_2	15.9	110	2.2
C_3	16	77	1.3

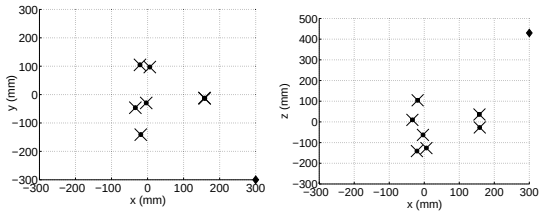

Figure 2: *Seven poses sets in the base frame, optimized with C_2 (crosses) and C_3 (circles) for the first measurement configuration. The camera center of projection is located in* $(300, -300, 430)$.

The seven poses are optimized according to the criteria C_2 and C_3 (Table 1). For this configuration, the optimized criteria values and poses are identical.

The calibration process is then simulated, using the optimized pose sets. For 1000 simulations, measurement noise is generated and added to the poses, before calibrating the structure. The average error vector E of the scaled parameters

$$E = Mean(\|\xi_{identified} - \xi_{model}\|)$$

are equal in this first measurement configuration.

4.3 Second measurement configuration

The working volume is here considered only delimited by the serial singularities. The noise increase with the distance is chosen five times higher than in the previous model, to simulate a lower quality sensor: the accuracy in the $\underline{\mathbf{x}}_\mathbf{C}$ and $\underline{\mathbf{y}}_\mathbf{C}$ directions varies between $0.18mm$ and $0.40mm$ in the workspace.

Now, the criteria values for the optimal pose sets are disparate: the optimal pose set according to C_3 has a 30% lower value of C_3 than the pose set optimized

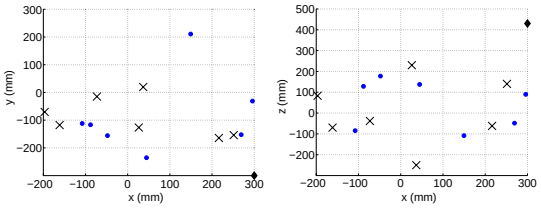

Figure 3: *Seven poses sets in the base frame, optimized with C_2 (crosses) and C_3 (circles), for the second measurement configuration. The camera center of projection is located in* $(300, -300, 430)$.

Table 2: *Criterion values for the 18 poses set.*

Kinematic chain	X-Axis	Y-Axis	Z-Axis
Value of C_3	312	286	366

according to C_2 (Table 1). The optimal pose set obtained with C_3 is closer (Figure 3) to the camera than the one obtained with C_2: the corresponding average distances between the poses and the camera are equal to $526mm$ and $570mm$.

Simulations confirm the need to take into account noise amplification using C_3: on 1000 simulations, the average error vector E is lowered by 41% using C_3 compared to the pose set optimized using the criterion C_2.

This example shows us that taking into account the noise propagation in the cost function through the use of C_3 may be necessary. It depends on the mechanism workspace used during the calibration and the measurement device. In this context, the simulation results indicate that the use of C_3 enables one a significant calibration improvement.

5 Experimentation

5.1 Pose selection

Six poses are necessary to identify the six kinematic parameters of each mechanism chain. To increase information redundancy, an eighteen poses set is optimized to perform the three kinematic chains calibration. The corresponding C_3 values are indicated in table 2. One may notice that the term $\|\delta\epsilon\|_{sup}$ is dependent on the number of poses. The indicated C_3 values are therefore not directly comparable to the values obtained for seven poses sets.

5.2 Kinematic calibration

An experimentation was conducted on the Orthoglide prototype (Figure 4), with fifty equally-spaced measured poses in the mechanism workspace. Among this pose set, the eighteen end-effector poses which are the

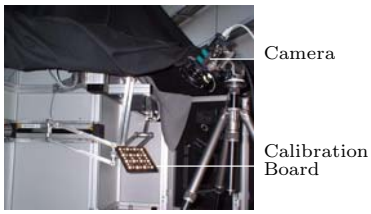

Figure 4: *Vision-based measuring device on the Orthoglide calibration.*

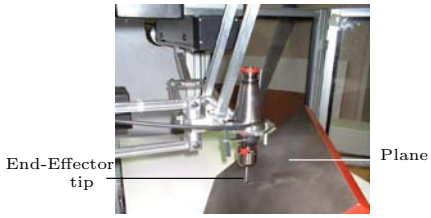

Figure 5: *Validation using a kinematic constraint.*

closest to the optimized ones are used for calibration. The experimentation conditions correspond to the first measurement configuration. No difference between the use of C_2 or C_3 can therefore be distinguished. To evaluate the calibration improvement bound to the use of an optimized pose set, the calibration is also performed 100 times using eighteen poses sets randomly selected among the fifty measurements.

5.3 Validation

The accuracy improvement is evaluated by an independent test. Indeed, the end-effector is manually constrained to follow a plane (Figure 5). The corresponding joint actuator encoder values are stored. Using either the *a priori* or identified parameters, the end-effector positions are computed using a numerical direct kinematic model. The physical set-up implies that these poses should lie on a plane. Hence, the identification efficiency is evaluated by computing the flatness of the plane as the root mean square of the distances between the different positions and the plane estimated by a least squares criterion.

Using the optimized pose set, a significant improvement of the flatness is observed, with a reduction from $0.23mm$ to $0.08mm$. The average flatness value obtained from the 100 randomly generated pose sets is equal to $0.1mm$, and the standard deviation equal to $0.02mm$. The use of an optimized pose set seeems to be favorable experimentally to the calibration efficiency.

6 Conclusion

In this paper, a pose selection criterion has been proposed for the kinematic calibration of parallel mechanisms based on the inverse kinematic model. It takes into account the measurement noise amplification that

may occur for such mechanisms, as well as the variation of amplitude and anisotropy of the measurement device accuracy. It allows one to use a least-squares identification cost function, as the *a priori* knowledge about the measurement errors may be insufficient to use a weighted least-squares cost function. This criterion is then used in the case of a vision-based calibration of an Orthoglide prototype. By simulation, the criterion efficiency has been outlined. It enables one to perform kinematic calibration with the minimal number of poses, for a constant accuracy improvement, hence reducing the experimental procedure.

The same pose selection strategy will now be applied for other mechanisms and also developed for calibration methods different from the inverse kinematic model method, such as the calibration by observation of the mechanism legs.

Acknowledgments

The authors would like to warmly thank S. Guégan, D. Chablat and P. Molina from IRCCyN for their help during the experiments. This study was jointly funded by CPER Auvergne 2001-2003 and by the CNRS-ROBEA program through the MAX project.

References

[1] J.-P. Merlet. *Parallel Robots*. Kluwer Academic Publishers, 2000. ISBN 0-7923-6308-6.

[2] J. Wang and O. Masory. On the accuracy of a Stewart platform - Part I: The effect of manufacturing tolerances. In *Proc. of ICRA93*, pages 114–120, 1993.

[3] H. Zhuang, J. Yan, and O. Masory. Calibration of Stewart platforms and other parallel manipulators by minimizing inverse kinematic residuals. *J. of Rob. Syst.*, 15(7):395–405, 1998.

[4] S. Besnard and W. Khalil. Identifiable parameters for parallel robots kinematic calibration. In *Proc of ICRA01*, pages 2859–2866, Seoul, Korea, 2001.

[5] M. Vincze, J.P. Prenninger, and H. Gander. A laser tracking system to measure position and orientation of robot end-effectors under motion. *Int. J. Rob. Res.*, 13(4):305–314, 1994.

[6] Z.J. Geng and L.S. Haynes. A "3-2-1" kinematic configuration of a Stewart platform and its application to six degrees of freedom pose measurements. *Robotics and Computer-Integrated Manufacturing*, 11(1):23–34, 1994.

[7] P. Renaud, N. Andreff, F. Marquet, and P. Martinet. Vision-based kinematic calibration of a H4 parallel mechanism. In *Proc. of ICRA03*, 2003. to appear.

[8] J. Swevers, C. Ganseman, B.D. Tükel, J. De Schutter, and H. Van Brussel. Optimal robot excitation and identification. *IEEE Trans. on Rob. and Autom.*, 13(5):730–740, 1997.

[9] D. Chablat and P. Wenger. Architecture optimization of a 3-DOF parallel mechanism for machining applications, the Orthoglide. *IEEE Trans. on Rob. and Autom.*, 2003. to appear.

[10] C.W. Wampler and J.M. Hollerbach. An implicit loop method for kinematic calibration and its application to closed-chain mechanisms. *IEEE Trans. on Rob. and Autom.*, 11(5):710–724, 1996.

[11] J.M. Hollerbach and C.W. Wampler. The calibration index and taxonomy for robot kinematic calibration methods. *The Int. J. of Rob. Res.*, 15(6):573–591, December 1996.

[12] K. Schroer. *Robot Calibration*, chapter Theory of kinematic modelling and numerical procedures for robot calibration, pages 157–196. Chapman & Hall, 1993.

[13] G. Zak, B. Benhabib, R.G. Fenton, and I. Saban. Aplication of the weighted least squares parameter estimation method to the robot calibration. *Trans. of the ASME*, 116:890–893, 1994.

[14] M.R. Driels and U.S. Pathre. Significance of observation strategy on the design of robot calibration experiments. *J. of Rob. Syst.*, 7(2):197–223, 1990.

[15] H. Zhuang, K. Wang, and Z. Roth. Optimal selection of measurement confgurations for robot calibration using simulated annealing. In *Proc. of ICRA94*, pages 393–398, 1994.

[16] D. Daney. Optimal measurement configurations for Gough platform calibration. In *Proc. of the ICRA02*, pages 147–152, Washington DC, 2002.

[17] J.H. Borm and C.H. Menq. Determination of optimal measurement configurations for robot calibration based on observability measure. *The Int. J. of Rob. Res.*, 10(1):51–63, 1991.

[18] A. Nahvi and J.M. Hollerbach. The noise amplification index for optimal pose selection in robot calibration. In *Proc. of ICRA96*, pages 647–654, Minneapolis, 1996.

[19] P. Renaud, N. Andreff, M. Dhome, and P. Martinet. Experimental evaluation of a vision-based measuring device for parallel machine-tool calibration. In *Proc. of IROS02*, Lausanne, October 2002.

[20] D. Chablat and P. Wenger. Working modes and aspects in fully manipulators. In *Proc. of ICRA98*, pages 1964–1969, Leuven, Belgium, May 1998.

[21] T. Mitchell. An algorithm for the construction of "D-optimal" experimental designs. *Technometrics*, 16(2):203–210, 1974.

[22] J.M. Lavest, M. Viala, and M. Dhome. Do we really need an accurate calibration pattern to achieve a reliable camera calibration. In *Proc. of ECCV98*, pages 158–174, Freiburg, June 1998.

[23] C. Innocenti. Polynomial solution of the spatial burmester problem. *Journal of Mechanical Design*, 117:64–68, 1995.